Check for updates

Batteries & Supercaps

Research Article
doi.org/10.1002/batt.202400031

Chemistry Europe
European Chemical Societies Publishing

www.batteries-supercaps.org

VIP *Very Important Paper*

Ultra-Long Lifespan Ni Based Porphyrin Complex Cathode for Organic Alkali Metal Batteries

Xi Peng[+],[a] Bo Ren[+],[a] Caihong Sun,[a] Yao Liao,[a] Fangfang He,[a] Tianfu Li,[a] Xiujuan Sun,[a] Zhi Chen,*[b] Wei Liu,*[c] and Ping Gao*[a]

The high solubility and low intrinsic electronic conductivity are the key challenges for application of organic materials in electrochemical energy storage. Herein, a functionalized porphyrin complex of [5,15-Bis(ethynyl)-10,20-diphenylporphinato]nickel(II) (NiDEPP) is proposed as new cathode material for alkali metal ion batteries. Owing to the in-situ electropolymerization, NiDEPP became extremely stable after initial cycling. Therefore, the NiDEPP electrode delivers remarkable reversible capacity of 153 mAh g^{-1} at 1 A g^{-1}, a high specific energy density of 459 Wh kg^{-1} and extremely stable cyclability for 4000 cycles with negligible capacity decay in organic lithium batteries. It can further be cycled upto 10000 cycles. Due to the bipolar capability of porphyrin ring, this cathode can also be extended in both sodium and potassium based organic cells. Similar charge storage mechanism enables highly reversible capacity and long-term cycling stability. This study would open a pathway toward new organic electrodes with long cycling life and high energy densities for renewable charge storage devices.

Introduction

Advances in energy storage technology have accelerated the wide application of rechargeable batteries in portable electronics, electric vehicles, and smart grids.[1] Lithium-ion batteries serve as the most widely employed electrochemical energy storage device. However, due to limited distribution of lithium resources in the earth crust and shortcomings in lithium recycling technology, alternatives to lithium resources are required. Consequently, considering the abundance of sodium and potassium resources, sodium-ion batteries (SIBs)[2] and potassium-ion batteries (KIBs),[3] have emerged as promising candidates for high performance energy storage. To promote higher storage capacity for alkali metal ion batteries requires constant development of suitable cathode materials. In the commercialization of alkali metal-ion batteries, inorganic materials such as layered transition metal oxides and phosphates are commonly used as electrode materials. However, the disadvantages of resource distribution, pollution, and safety concerns, limits the further development of inorganic materials, particularly for the renewable energy storage.

Organic electrode materials have shown great potential for sustainable charge storage devices to substitute inorganic electrode materials in alkali metal-ion batteries due to their low cost, abundant resource, tunable performance, and environmental friendliness.[4] Up to now, many organic compounds have been proposed as electrode materials, such as carbonyl compounds,[5] organic sulfides,[6] and conductive polymers.[7] Nevertheless, the high solubility in electrolytes and low intrinsic electronic conductivity are the key challenges for the development of organic electrode materials. Strategies such as polymerization,[8] funcationalized groups[9] and modification of electrolytes[10] were efficient approaches for addressing partial issues above. However, there is still lack of organic materials which are capable of high energy density, power density and cycling stability. Hence, new functional organic electrode materials are needed to be explored by molecular engineering or learning from nature. Porphyrin, a macromolecular heterocyclic compound with 18π electron conjugation among the four pyrrole groups, is widely utilized in the fields of catalysis and organic photovoltaics.[11] Their small highest occupied molecular orbital (HOMO)-lowest unoccupied molecular orbital (LUMO) gaps that enable fast electron uptake and release,[12] porphyrins exhibit high redox activities. In recent years, porphyrin-based redox active materials have emerged as a novel type of electrochemical energy storage organic electrode for supercapacitors[13] and rechargeable batteries.[14] Porphyrin derivatives have demonstrated remarkable electrochemical performance in alkali metal ion batteries, multivalent metal ion batteries,[15] lithium-sulfur batteries,[16] and redox flow batteries.[17] Furthermore, porphyrin-based COF[18] and MOF[19] materials were also proposed as active materials in rechargeable battery systems due to the highly ordered structure. GAO et al[20] conducted a systematic investigation on the influence of

[a] X. Peng,[+] B. Ren,[+] C. Sun, Y. Liao, F. He, T. Li, X. Sun, Prof. Dr. P. Gao
Key laboratory of Enviromentally Friendly Chemistry and Application of Ministry of Education, College of Chemistry,
Xiangtan University, 411105, Xiangtan, China
E-mail: ping.gao@xtu.edu.cn

[b] Dr. Z. Chen
Collge of Chemistry and Environmental Engineering, Shenzhen University, Shenzhen, Guangdong, 518060, China
E-mail: zhi.chen@szu.edu.cn

[c] Dr. W. Liu
Yiyang Hongyuan Rare Earth Co., Ltd, Yiyang 413001, China
E-mail: 332096904@qq.com

[+] These authors contributed equally

Supporting information for this article is available on the WWW under https://doi.org/10.1002/batt.202400031

© 2024 Wiley-VCH GmbH

Research Article
doi.org/10.1002/batt.202400031
Chemistry Europe
European Chemical Societies Publishing

different coordination meso-functional groups, coordination metal centers, various electrolytes, and temperature on the electrochemical properties of porphyrins. The bipolar property of porphyrin ring enables a four-electron transfer during the redox process, resulting in high energy and power density. The acetylenic group and the phenyl group that modified porphyrin complexes can reduce the solubility of active material and lead to fast redox reactivity by electropolymerization and expanding the π-conjugated structure, respectively. This molecular engineering strategy may lead to impressive capacity retention and high specific discharge capacity in alkali metal ion batteries. Besides organometallic complexes possess dual functional properties of organic and inorganic moieties, which can be potential for charge storage.[21] Shin et al. reported the dimesitylnorcorrole nickel(II) complex as an electrode material, it delivered high discharge voltage and capacity,[22] where highly reversible capacity and good cycling stability was achieved.

In this study, we aim to investigate the charge storage of [5,15-Bis(ethynyl)-10,20-diphenylporphinato]nickel(II) (NiDEPP) molecules in alkali metal ion batteries ($Li^+/Na^+/K^+$ based organic batteries) and explore the reaction mechanisms during electrochemical processes. Figure 1a–b illustrates the proposed schematic of electron transfer of NiDEPP cathode during charging and discharging processes. The detailed charge storage capability and reaction mechanism of NiDEPP are systematically evaluated through different spectroscopic and microscopic techniques.

Results and Discussion

Details for the synthesis of NiDEPP are provided in experimental section and Scheme S1. Scanning electron microscopy (SEM) revealed that the obtained NiDEPP solids are rod-shaped crystals with an average length of approximately 25 μm and a width of 5 μm (Figure 1c and S6). The elemental mapping images of NiDEPP (Figure 1d–f) carried out by the EDX analysis, which showed the uniform distribution of C, N, Ni elements. The X-ray diffraction (XRD) pattern (Figure 1g) indicates the

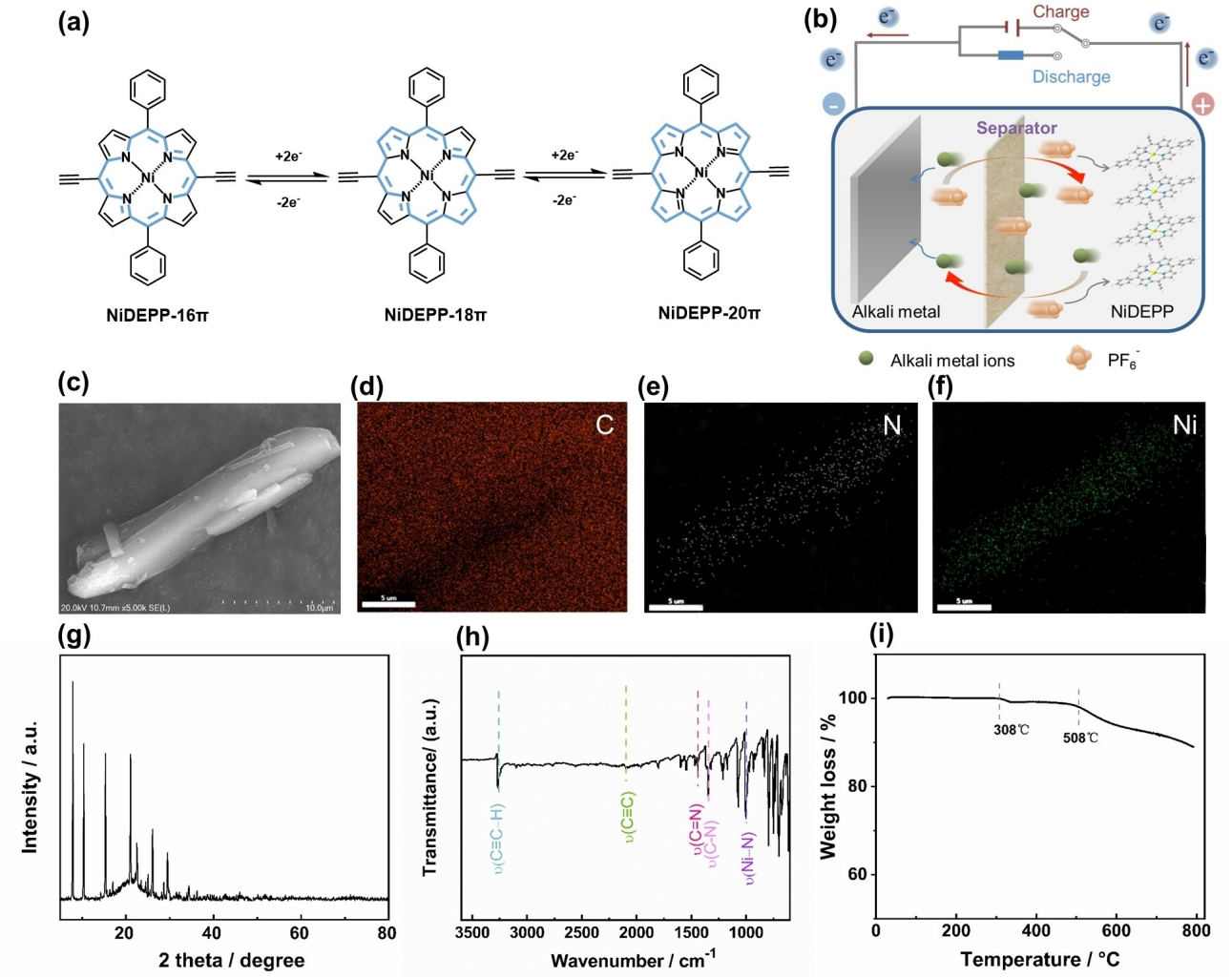

Figure 1. (a)Working principle of NiDEPP during the charge and discharge process. (b)Schematic illustration of NiDEPP cathode during charging and discharge process, alkali metal ions are Li^+, Na^+, K^+. (c) SEM image, and elemental mapping images of (d) C, (e) N and (f) Ni for NiDEPP (scale bars denote 5 μm). (g) XRD pattern of NiDEPP. (h) the IR spectra of NiDEPP in the range of 600–3600 cm^{-1}. (i) TG result of NiDEPP.

© 2024 Wiley-VCH GmbH

25666223, 2024, 5, Downloaded from https://chemistry-europe.onlinelibrary.wiley.com/doi/10.1002/batt.202400031 by University of Ulsan, Wiley Online Library on [11/11/2025]. See the Terms and Conditions (https://onlinelibrary.wiley.com/terms-and-conditions) on Wiley Online Library for rules of use; OA articles are governed by the applicable Creative Commons License

Research Article
doi.org/10.1002/batt.202400031
Chemistry Europe
European Chemical Societies Publishing

highly crystalline nature of NiDEPP sample. The ATR-FTIR test was carried out in the range from 600 to 3600 cm^{-1} (Figure 1h). The characteristic peaks at 3260 cm^{-1} and 2090 cm^{-1} belong to –C≡C–H and –C≡C–, respectively. The peak at 1440 cm^{-1} is ascribed to –C=N of porphyrin, and the stretching vibration of C–N appears at 1340 cm^{-1}. The characteristic peak of Ni–N bond absorption appears at 1006 cm^{-1}. The thermal decomposition test of NiDEPP indicates that the molecule can be stable up to 308 °C in N_2 (Figure 1i). This good thermal stability can be related to its strong intermolecular π-π stacking of porphyrin complex, which makes it possible to demonstrate good cycling stability in alkali metal batteries at high temperature.

To understand the charge storage characteristics of NiDEPP, the cycling and rate performance were systematically studied. Firstly, the electrochemical performance of NiDEPP (50 wt% of the total mass electrode) was initially evaluated in Li-ion based half-cell, in which NiDEPP was used as a cathode, Li foil was used as an anode. The cyclic voltammetry (CV) was tested in a voltage range of 1.8–4.5 V (vs. Li^+/Li) at a scan rate of 0.1 mV s^{-1}. During the first anodic scan, a distinct irreversible oxidation peak appeared at 4.2 V (Figure 2a), which is consistent

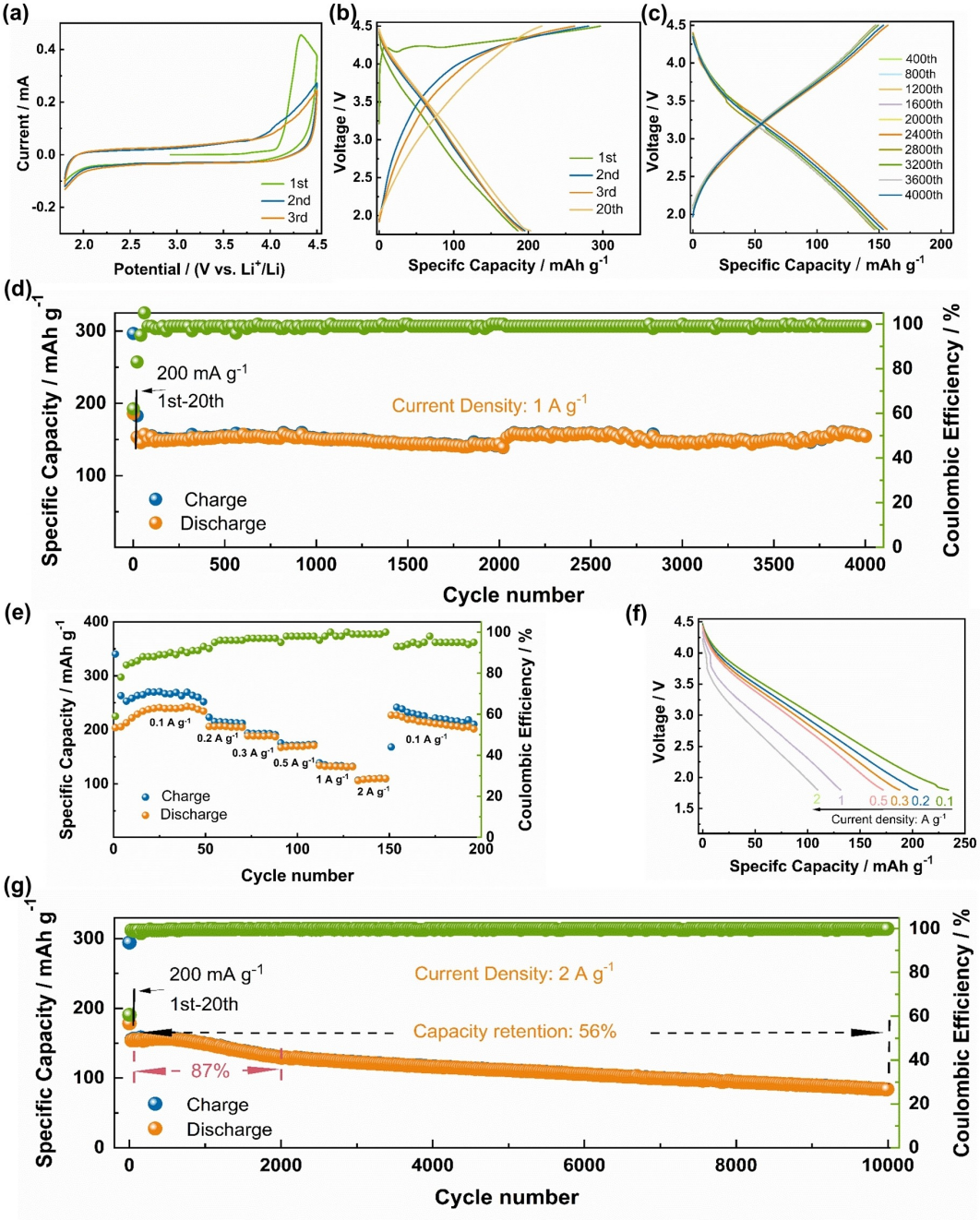

Figure 2. (a)CV curves of NiDEPP cathode at the scanning rate of 0.1 mV s^{-1}. (b)The charge-discharge curves at different cycles at 0.2 A g^{-1}. (c)Selected charge-discharge curves at 1 A g^{-1}. (d) Cycling performance at 1 A g^{-1}. (e) rate performance of NiDEPP. (f) Selected discharge curves of (e), (g) long-term cycling performance of NiDEPP at 2 A $g^{yM->1}$.

© 2024 Wiley-VCH GmbH

25666223, 2024, 5, Downloaded from https://chemistry-europe.onlinelibrary.wiley.com/doi/10.1002/batt.202400031 by University of Ulsan, Wiley Online Library on [11/11/2025]. See the Terms and Conditions (https://onlinelibrary.wiley.com/terms-and-conditions) on Wiley Online Library for rules of use; OA articles are governed by the applicable Creative Commons License

Research Article
doi.org/10.1002/batt.202400031
Chemistry Europe
European Chemical Societies Publishing

with a flat voltage plateau at 4.2 V during the first charging (Figure 2b). This process is resulted from the electropolymerization of ethynyl groups of the porphyrin molecules and the interaction of PF_6^- anion with NiDEPP cathode. There are no significant redox peaks in the following electrochemical progress. Sloping curve without charge voltage plateau was observed in the subsequent cycles, indicating that the charge storage mechanism may be related to a fast kinetic process and the NiDEPP-based charge storage was similar to that of supercapacitors, will be discussed later. The voltage range of 1.8–4.5 V was utilized in the galvanostatic charge/discharge (GCD) at a current density of 200 mA g^{-1}. In the first cycle, the charge and discharge capacities of 297 mAh g^{-1} and 185 mAh g^{-1} were obtained (based on the mass of active material) for NiDEPP cathode, respectively, which was close to the theoretical value of 189 mAh g^{-1} based on four-electron transfer ($[NiDEPP]^{2+} \leftrightarrow [NiDEPP]^{2-}$).

The cycling stability of NiDEPP was evaluated at current density of 1 A g^{-1} between 1.8 V to 4.5 V (vs. Li^+/Li). The cell was initially cycled at a low current density of 200 mA g^{-1} for 20 cycles, which could provide better condition for NiDEPP at a high rate. Discharge specific capacity of 203 mAh g^{-1} was achieved in the 20th cycle. In the following cycles at 1 A g^{-1}, the charge/discharge curves were overlapped with a discharge capacity of 153 mAh g^{-1}, indicating the highly reversible capacity of NiDEPP (Figure 2c). Furthermore, an average discharge voltage up to 3.0 V was achieved with an energy density of 459 Wh kg^{-1}. NiDEPP showed extremely cycling stability up to 4000 cycles. Capacity retention of 99.88% was obtained within 4000 cycles with coulombic efficiency close to 100% (Figure 2d). In addition to the excellent cycling performance, the rate performance of NiDEPP was further tested from 0.1 to 2 A g^{-1} (initial 50 cycles at 0.1 A g^{-1}, from 0.2 to 2 A g^{-1}, 20 cycles for each current density). The NiDEPP cathode delivered discharge specific capacities of 234, 204, 187, 172, 131 and 109 mAh g^{-1} at 0.1, 0.2, 0.3, 0.5, 1.0, and 2.0 A g^{-1}, respectively (Figure 2e). The discharge capacity corresponded to 86% of the capacity at the initial current density of 0.1 A g^{-1} when the current density was back from 2.0 to 0.1 A g^{-1}, exhibiting remarkable reversibility during the electrochemical reaction. In the comparison of the selected discharge profiles at different current density, the over potential and electrode polarization were subtly increased with increasing of current density (Figure 2f). To further understand the fast charge-discharge capability, the cell was operated at a high current density of 2.0 A g^{-1} (Figure 2 g). The NiDEPP delivered a maximum capacity of 156 mAh g^{-1} in the 535th cycle after initial cycles at 0.2 A g^{-1}. The capacity retention of 87% and 56% was obtained for 2,000 and 10,000 cycles, respectively. This good cycling stability at a high current density can be ascribed to the good electron transfer path, fast charge mobility and stable structure of NiDEPP electrode during charging/discharging process. Due to the bipolar capability of porphyrin complex, different cations and anions would also be stored during the electrochemical reaction.

To better evaluated the widespread application of NiDEPP in organic alkali metal batteries, we further investigated the electrochemical performance of NiDEPP electrode in sodium-ion (SIBs) and potassium-ion (PIBs) based batteries. Similar to lithium-based system, NiDEPP was used as the cathode, while Na (K metal) foil was used as the anode. As shown that NiDEPP electrode demonstrated good charge storage performance and excellent cycling stability in Li-ion battery, to further test in sodium-based system. The initial galvanostatic charge/discharge (GCD) was tested at a current density of 0.2 A g^{-1} in a voltage range of 1.8–4.5 V (vs Na^+/Na). Owing to the electropolymerization process and the anion of electrolyte interaction with NiDEPP, the initial charge curve showed a slope voltage plateau at 4.0 V (Figure 3a). This indicates that the charge storage mechanism of NiDEPP in sodium-ion batteries is similar to that in lithium-based system. The NiDEPP cathode showed a highly reversible the discharge capacity of 162 mAh g^{-1} at a current density of 200 mA g^{-1} after 100 cycles. When it was operated at a higher current density of 500 mA g^{-1}, the discharge capacity of 127 mAh g^{-1} and capacity retentions of 90% were achieved for 800 cycles (Figure 3b). The semblable charge/discharge curves in following cycles demonstrated excellent cycling stability (Figure 3c). To further investigate the rate capability of NiDEPP in SIBs (Figure S7a). At different current density of 0.1, 0.2, 0.3, 0.5, 1.0, and 2.0 A g^{-1}, the NiDEPP delivered reversible discharge capacities of 88, 57, 47, 37, 27 and 17 mAh g^{-1}, respectively. When the current density was

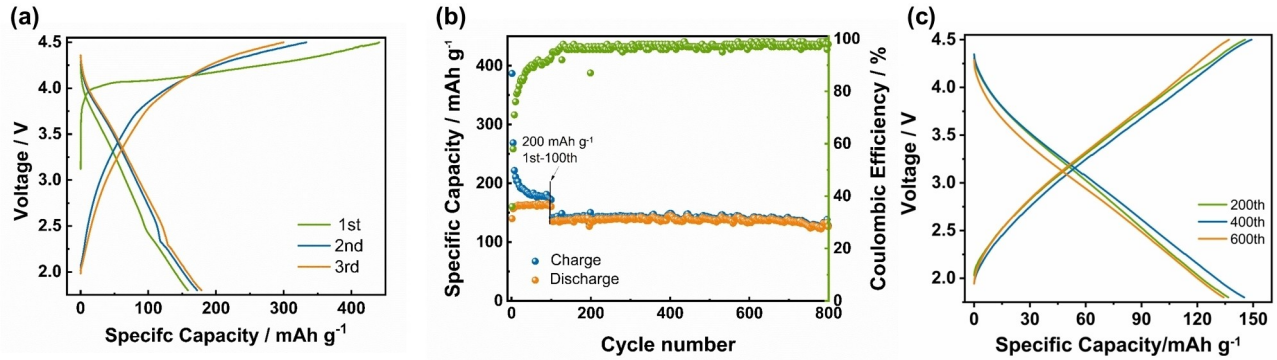

Figure 3. (a)Initial charge-discharge curve of NiDEPP at 0.2 A g^{-1}, (b) Cycling performance of NiDEPP at 0.5 A g^{-1}, (c) Selected charge-discharge profiles at 0.5 A g^{-1}.

© 2024 Wiley-VCH GmbH

25666223, 2024, 5, Downloaded from https://chemistry-europe.onlinelibrary.wiley.com/doi/10.1002/batt.202400031 by University of Ulsan, Wiley Online Library on [11/11/2025]. See the Terms and Conditions (https://onlinelibrary.wiley.com/terms-and-conditions) on Wiley Online Library for rules of use; OA articles are governed by the applicable Creative Commons License

Research Article
doi.org/10.1002/batt.202400031
Chemistry Europe
European Chemical Societies Publishing

tuned from 2.0 to 0.1 A g^{-1}, the discharge capacity returned to the previous value (88 mAh g^{-1}), but it showed a significant decrease, which may be related to the irreversible insertion and desorption of large diameter sodium ions. In Figure S7b, the discharge curves with different current densities, suggest that the over potential and polarization of NiDEPP in sodium ion batteries were slightly increased with increasing of current density.

In addition, based on the result of charge storage in lithium and sodium-based system, NiDEPP could also be possible for K ion storage. Therefore, the cycling performance of NiDEPP cathode was also tested, where potassium metal was used as anode. As it is displayed in Figure 4a, at a current density of 300 mA g^{-1} in the voltage range of 1.7-4.4 V, which a voltage plateau located at 4.2 V during the first charge, which was consistent with the case in Li and Na. The discharge capacity stabilized at 118 mAh g^{-1} in initial three cycles with an average discharge voltage of 2.9 V. The discharge capacity increased to 147 mAh g^{-1} in the 100th cycle, the capacity retention of 96% for the 300 cycles, and the parallel charge/discharge curves in different cycles indicating the good cycling stability of NiDEPP in potassium-based batteries as well (Figure 4b–c). These results indicated that the highly reversible capacity can be achieved with different cations and anions stored in NiDEPP cathode, implying the universal charge storage capability of NiDEPP cathode. Nevertheless, the coulombic efficiency and cycling stability of NiDEPP in various alkali metal batteries are different. This probably resulted from the reactive activity of the alkali metal, the dendritic growth, the stability of the solid electrolyte interface (SEI), and the volume change of the electrodes. To overcome the issue, various strategies, including tailoring electrolyte formulation, artificial SEI, and modifying electrode structures are proposed in the subsequent work.

In order to gain in-depth understanding the electrochemical performance and storage mechanism of the NiDEPP electrode, we conducted post-mortem analysis by means of ex situ X-ray photoelectron spectroscopy (XPS), scanning electron microscopy (SEM), ex situ X-ray diffraction (XRD), Fourier transform infrared (FTIR) spectroscopy, ex-situ Raman spectra, and UV-Vis spectroscopy. The stretching band at 3269 cm^{-1} and the vibration band at 2106 cm^{-1} corresponded to –C≡C–H and –C≡C– of ethynyl group of the NiDEPP, respectively (Figure 5b). These two peaks gradually weakened after initial cycles, which implies that electropolymerization of the ethynyl group on NiDEPP was occurred during the charge and discharge processes. In the charged state, a new peak of P–F appeared at 835 cm^{-1}, which confirmed that the anion PF_6^- in the electrolyte was absorbed on NiDEPP during charging. However, this peak

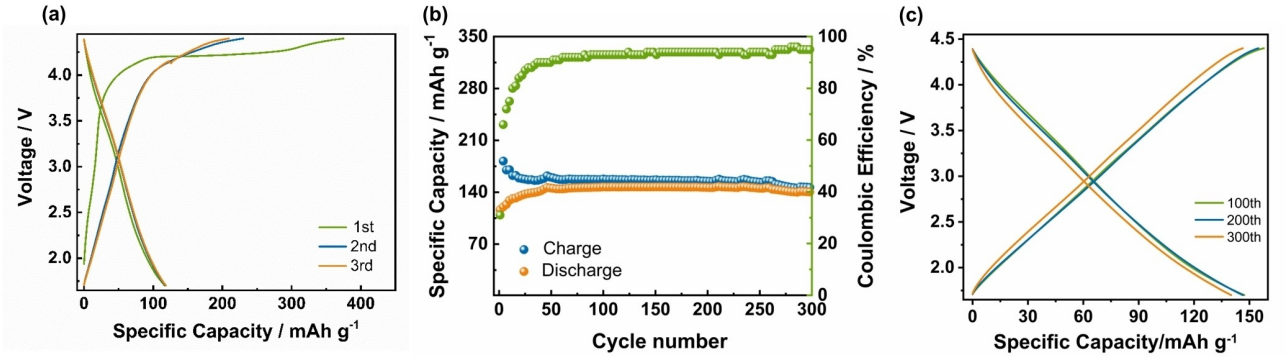

Figure 4. (a)Initial charge-discharge curve of NiDEPP at 0.3 A g^{-1}. (b) Cycling performance of NiDEPP at 0.3 A g^{-1}. (c) Selected charge-discharge curves of NiDEPP at 0.3 A g^{-1}.

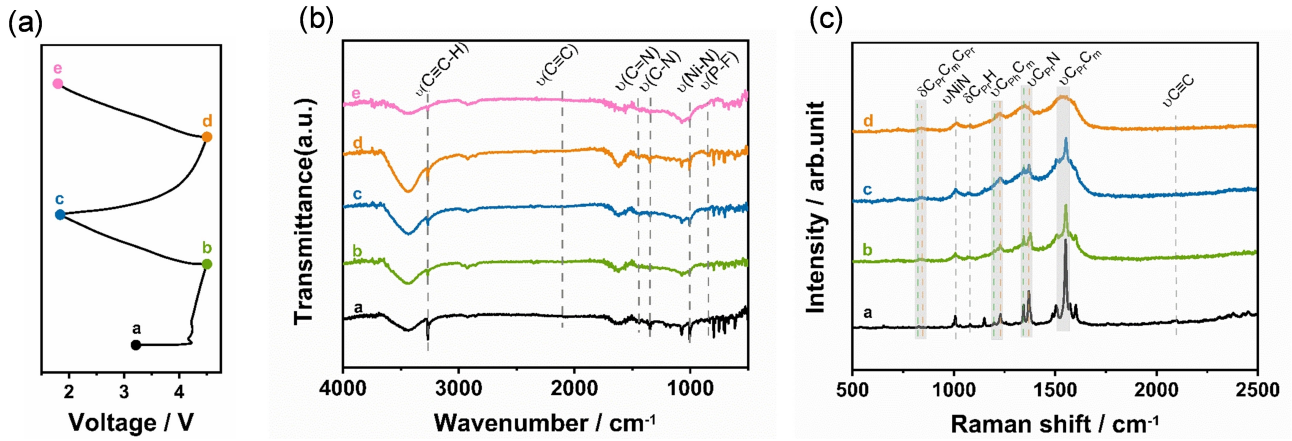

Figure 5. (a)Initial charge/discharge profiles of NiDEPP cathodes. (b) Ex situ FTIR of NiDEPP. (c) Raman spectra of NiDEPP. (a: pristine, b: charged to 4.5 V, c: discharged to 1.8 V, d: re-charged to 4.5 V, e: re-discharged to 1.8 V).

© 2024 Wiley-VCH GmbH

25666223, 2024, 5, Downloaded from https://chemistry-europe.onlinelibrary.wiley.com/doi/10.1002/batt.202400031 by University of Ulsan, Wiley Online Library on [11/11/2025]. See the Terms and Conditions (https://onlinelibrary.wiley.com/terms-and-conditions) on Wiley Online Library for rules of use; OA articles are governed by the applicable Creative Commons License

Research Article
doi.org/10.1002/batt.202400031
Chemistry Europe
European Chemical Societies Publishing

did not fully vanish in the subsequent discharge step, proving a slightly irreversible process. Meanwhile, the vibration peak of porphyrin at 1006 cm^{-1} assigned to Ni–N remained in the charged and discharged states compared with the as-prepared state, which suggests that the interaction of N atoms and PF_6^- can significantly affect the vibration of Ni–N bond. During charging and discharging, both the C=N at 1442 cm^{-1} and the C–N absorption peak at 1348 cm^{-1} of NiDEPP started to weaken and gradually merged into a broaden peak, proving that nitrogen atoms of porphyrin molecule acted as the charge storage site for PF_6^-.

Furthermore, the corresponding ex-situ Raman spectra of the NiDEPP electrode under different voltages are shown in Figure 5c. The assignments of the bands are provided in Table S1. The Ni–N band at 1006 cm^{-1} broadened in the fully charged and discharged states, which was similar to the result of FTIR. The peaks of the $C_{Pr}N$ at 1344 cm^{-1} and 1369 cm^{-1} merged into a single peak, which further confirms that N atoms acted as the active sites of the NiDEPP. After cycling, the stretching peak of $C_{Pr}C_m$ broadened at 1522 cm^{-1}. The disappearance of the vibrational peak of the –C≡C– group at 2098 cm^{-1} indicated that the porphyrin electropolymerized through the ethynyl group during the initial cycle, which was consistent with the IR results. Due to the polymerization upon cycling, the solubility of NiDEPP electrode in THF and PC and the value of the absorbance at Soret and Q bands were progressively reduced (Figure S8), which was consistent with the IR and Raman results.

XPS spectra were also carried out to understand the charge storage reaction mechanism of the NiDEPP electrode. The full survey spectra of different cycled NiDEPP indicates that carbon, nitrogen, nickel of porphyrin complex as well as elements of the electrolyte were detected (Figure 6a). In the as-prepared NiDEPP, the characteristic N 1s with a binding energy at 399.1 eV assigned to –C=N– was detected, while peak with binding energy at 400.6 eV stood for –C–N–, respectively (Figure 6b). When charged to 4.5 V, the binding energy of N 1s shifted to a lower energy level. The N 1s peak assigned to –C–N– returned to its original position upon discharging to 3.0 V, indicating that the aromatic porphyrin molecule (18π) was oxidized to 16π and then reduced to 18π in this process. It simultaneously certified that the PF_6^- anion interacted with nitrogen atoms of porphyrin leading to the variation of N 1 s. When it was discharged to 1.8 V, the N 1s characteristic peaks were shifted to the lower energy at 398.9 and 400.1 eV again, and the areas of the –C=N– and –C–N– peaks were similar in size, indicating that the porphyrin ring of NiDEPP was reduced to 20 π, and the storage site of Li^+ cation was nitrogen atom during the discharge process. When it was recharged to 4.5 V, characteristic peaks of N 1s were remained, indicating that the electrochemical reaction is reversible in the NiDEPP. These variations further suggested that the nitrogen atoms on NiDEPP are the active sites for binding with the anions and cations, and two species of ions contribute equally to the charge storage based on two electrons oxidation and two electrons reduction mechanism. In the Figure 6c, the characteristic F 1s of the pristine sample with a binding energy at 688.6 eV corresponds to the C–F in PVDF. Upon charging, a new peak with binding energy at 685.9 eV appeared apart from the F 1s main peak, which indicated the reaction of the electrolytes with NiDEPP to form the LiF. Furthermore, the peak assigned to LiF was remained during subsequent cycles, proving the formation of

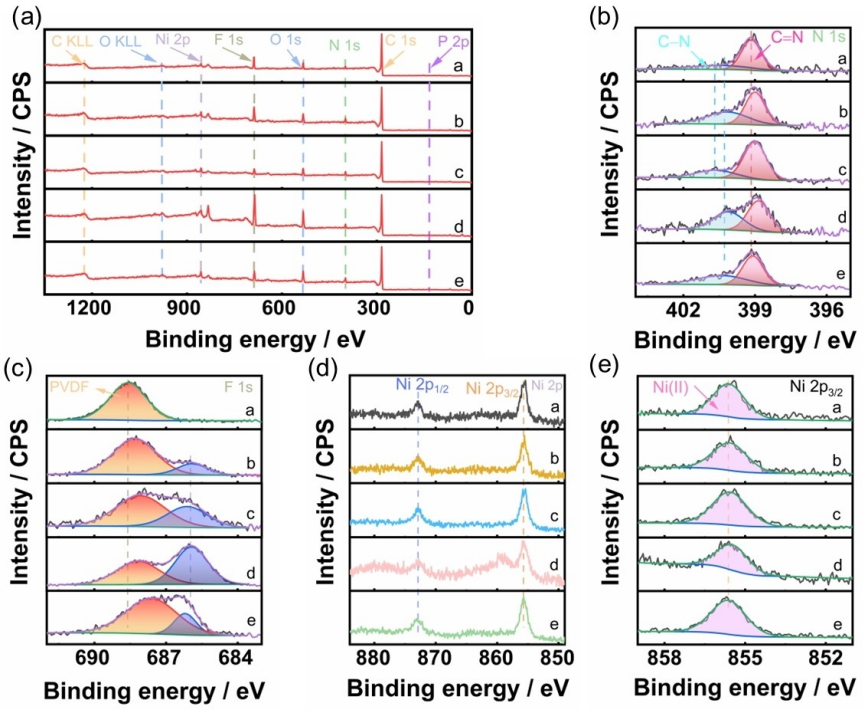

Figure 6. (a)Survey XP spectra of NiDEPP at different charged states. (b) XP spectra core level of N1 s, (c) F1s, (d) Ni 2p, (e) Ni $2p_{3/2}$ of NiDEPP in different states. (a: pristine, b: charged to 4.5 V, c: discharged to 3.0 V, d: discharged to 1.8 V, e: recharged to 4.5 V)

© 2024 Wiley-VCH GmbH

25666223, 2024, 5, Downloaded from https://chemistry-europe.onlinelibrary.wiley.com/doi/10.1002/batt.202400031 by University of Ulsan, Wiley Online Library on [11/11/2025]. See the Terms and Conditions (https://onlinelibrary.wiley.com/terms-and-conditions) on Wiley Online Library for rules of use; OA articles are governed by the applicable Creative Commons License

the stable cathode-electrolyte interface in the initial reaction. Binding energies for Ni 2p at 855.6 eV (Ni $2p_{3/2}$) and 873.0 eV (Ni $2p_{1/2}$) were observed (Figure 6d and e), which can be ascribed to divalent nickel in NiDEPP. It is noticed that no significant change in the binding energy for Ni was observed during the cycles, which indicated that the central metal ion Ni^{2+} did not participate in the charge storage. The role of Ni^{2+} was more beneficial for the stabilization of the porphyrin structure than Cu^{2+}, which would be involved in the reaction.[20a,22] This finding agreed well with the result that the shape of the NiDEPP as regular long strips was remained during 2000 cycles (Figure S9), which greatly ensuring ultra-long lifespan of cycling performance.

A more detailed investigation of the fast kinetics for charging/discharging the NiDEPP cathodes was performed via CV measurements at different scan rates from 0.1-3.0 $mV\,s^{-1}$ (Figure 7a). Using the method proposed by Dunn and colleagues, the peak current (i) and scan rate (v) obeyed a power-law relationship, $i = av^b$, where a and b were adjustable constants. The fitted b-values of anodic and cathodic scans of NiDEPP were 0.87 and 0.99, respectively, suggesting that a mixture process dominated by the surface-controlled processes (Figure 7b). Quantification of the surface-controlled contribution ratios was done using formula: $i = k_1v + k_2v^{1/2}$, where, k_1, k_2 were two constants, v was the scan rate, and k_1v, $k_2v^{1/2}$ represented the surface-controlled (pseudocapacitive) and diffusion-controlled portion, respectively. As the scan rate increased from 0.1 $mV\,s^{-1}$ to 3.0 $mV\,s^{-1}$, the pseudocapacitance contributions increased from 70% to 93%, indicating that the pseudocapacitance behavior plays a dominant role in the capacitive contribution (Figure 7c). Electrochemical impedance spectroscopy (EIS) was used to further investigate the resistance variation of the porphyrin during cycling. The charge transfer resistance of the NiDEPP electrode increased during the initial fifth cycle (Figure S10a), which may be related to the formation of the electrolyte interface film. After the fifth cycle, the resistance was significantly reduced, which suggested that the polymerization of NiDEPP during initial cycling can stabilize the electrode interface, reduce the charge transfer resistance, thus allowing for fast kinetics during the following cycling process (Figure S10b).

Encouraged by reversible capacity and the high discharge voltage of the NiDEPP as cathode in a half-cell, a lithium-free NiDEPP/PP_{14}TFSI/graphite cell was constructed to further test the electrochemical capability in the potential application. The schematic diagram of cell during charging process is shown in Figure 8a. The graphite was used as a cathode, the NiDEPP was used as an anode. It should be noted that pure ionic liquid of PP_{14}TFSI was used as an electrolyte, where only PP_{14}^+ and $TFSI^-$ shuttles during cycling, no solvent is involved. The full cell delivered an initial reversible capacity of 91 $mAh\,g^{-1}$(based on the weight of the NiDEPP) at 0.5 $A\,g^{-1}$ (Figure 8b). Charge and discharge curves were overlapped after the first cycle, indicating highly reversible. When the cell was cycled at a high current density of 1.0 $A\,g^{-1}$, a discharge capacity of 55 $mAh\,g^{-1}$ was still obtained after 300 cycles with a capacity retention of 60%, implying the combination of NiDEPP and graphite for a full cell can demonstrate good electrochemical charge storage performance (Figure 8c).

Conclusions

In summary, a functionalized porphyrin complex of [5,15-bis(ethyl)-10,20-diphenylporphinato] nickel(II) (NiDEPP) is proposed as a new electrode for rechargeable energy storage devices. It is noticed that the NiDEPP can interact with different alkali metal ions (Li^+, Na^+, K^+), showing good charge storage performance. The NiDEPP cathode delivers a discharge specific capacity of 153 $mAh\,g^{-1}$ after 4000 cycles with a capacity retention of 99.87% in a lithium-based cell. An energy density of 459 $Wh\,kg^{-1}$ is achieved. In organic sodium and potassium batteries, NiDEPP cathode also demonstrated highly reversible capability and cycling stability up to 800 and 300 cycles are achieved in a half cell. Highly stable performance is also demonstrated in a full cell coupled with a graphite cathode. Charge storage mechanism is systematically evaluated using different ex-situ spectra techniques, supporting the alternative storage of both anions and cations with porphyrin molecule. This study would provide a new strategy for the development of new organic materials for alkali metal ion batteries.

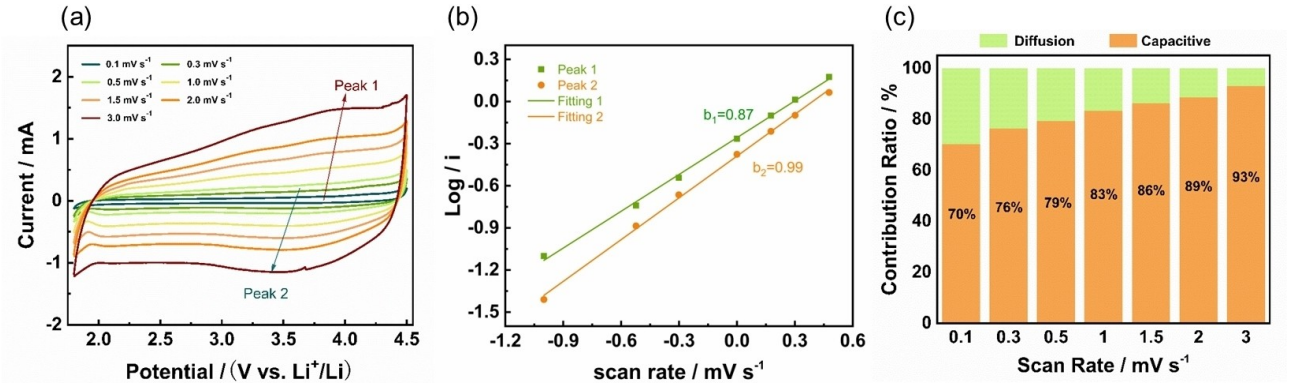

Figure 7. (a) CV curves at different scan rates. (b) The corresponding plots log (i) versus log (v) at each redox peak. (c) The capacitive contribution ratio at different scan rates.

© 2024 Wiley-VCH GmbH

25666223, 2024, 5, Downloaded from https://chemistry-europe.onlinelibrary.wiley.com/doi/10.1002/batt.202400031 by University of Ulsan, Wiley Online Library on [11/11/2025]. See the Terms and Conditions (https://onlinelibrary.wiley.com/terms-and-conditions) on Wiley Online Library for rules of use; OA articles are governed by the applicable Creative Commons License

Research Article
doi.org/10.1002/batt.202400031
Chemistry Europe
European Chemical Societies Publishing

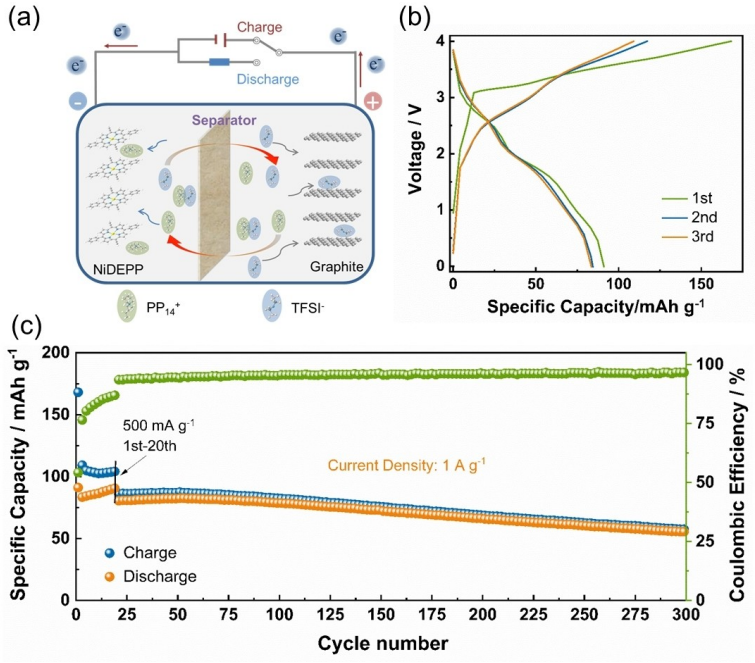

Figure 8. (a)Schematic diagram of NiDEPP/PP_{14}TFSI/Graphite cell during charging process. (b) The initial charge/discharge profiles of the full cell at 0.5 A g^{-1}. (c) Cycling performance of the full cell. The cell was cycled at 0.5 A g^{-1} for initial 20 cycles, and at 1 A g^{-1} for additional 280 cycles in a voltage range of 4.0–0.0 V.

Experimental Section

Materials Preparation

The detailed synthesis scheme of NiDEPP is shown in the Supporting Information. The cathodes were prepared by mixing the active materials (NiDEPP), actylene black, PVDF binder at a mass ratio of 5:4:1 in NMP. After that, the slurry was cast on the stainless steel foil and dried in vacuum at 110°C for 12 h before use. The NiDEPP was used as cathode; Li, Na and K metal were used as anode and 1 M lithium hexafluorophosphate ($LiPF_6$) in propylene carbonate (PC), 1 M sodium hexafluorophosphate ($NaPF_6$) in a mixture of PC and 5 wt% fluoroethylene carbonate (FEC), and 1 M potassium hexafluorophosphate (KPF_6) in dimethoxyethane (DME) or PC were used as electrolytes to assemble half-cells. Whatman glass fiber was used as the separator. The average mass loading of NiDEPP was around 1.25 mg cm^{-2}. All capacities were calculated based on the active material of the electrode.

Materials Characterization

^{1}H and ^{13}C NMR spectra were recorded with a Bruker Avance 400 instrument. Mass spectrometry (MS) was performed on a Bruker Aupoflflex III MALDI-TOF Analyzer using CCA as matrix. The morphology and elemental analysis were observed using a field emission scanning electron microscope (FESEM, ZEISS LEO 1530) and an energy dispersive X-ray spectroscopy (EDX) with an X–Max Silicon Drift Detector. Powder X-ray diffraction (XRD) patterns were recorded using a D8 ADVANCE X-ray diffractometer with a Cu Ka radiation source ($\lambda = 0.154$ nm). UV-vis spectra of porphyrins were measured on a Perkin–Elmer Cary 60 spectrometer. The attenuated total reflectance-fourier transformation infrared (ATR-FTIR) spectrum was recorded using a Thermo Fisher Nicolet IS50 spectrometer between 600 and 4000 cm^{-1}. The thermogravimetry–differential scanning (TGA) was recorded on a Netzsch TG 209 (Netzsch). The Raman spectra was tested by a Raman instrument (In Via, Renishaw) and the laser wavelength is 532 nm. X-ray photoelectron spectroscopy (XPS) was recorded on a Escalab250Xi (Thermo Scientific) by using monochromatized Al Kα radiation (1486 eV). The pass energy for survey spectra was 100 eV, for detail spectra the energy was 30 eV. The binding energies of all spectra were calibrated with respect to the C1s peak of ubiquitous carbon at a binding energy of 284.8 eV.

Acknowledgements

This work was financially supported by National Natural Science Foundation of China (22279109, 22101181), Natural Science Foundation of Hunan Province (2022JJ20036), and Scientific Research Fund of Hunan Provincial Education Department (23B0114). Xi Peng and Bo Ren contributed equally to this work.

Conflict of Interests

The authors declare no conflict of interest.

Data Availability Statement

The data that support the findings of this study are available in the supplementary material of this article.

Keywords: organic material · alkali metal batteries · ultra-long lifespan

© 2024 Wiley-VCH GmbH

25666223, 2024, 5, Downloaded from https://chemistry-europe.onlinelibrary.wiley.com/doi/10.1002/batt.202400031 by University of Ulsan, Wiley Online Library on [11/11/2025]. See the Terms and Conditions (https://onlinelibrary.wiley.com/terms-and-conditions) on Wiley Online Library for rules of use; OA articles are governed by the applicable Creative Commons License

[1] Y. Liang, C. Luo, F. Wang, S. Hou, S. C. Liou, T. Qing, Q. Li, J. Zheng, C. Cui, C. Wang, *Adv. Energy Mater.* **2018**, *9*, 1802986.
[2] a) J. Qian, X. Wu, Y. Cao, X. Ai, H. Yang, *Angew. Chem. Int. Ed. Engl.* **2013**, *52*, 4633–4636; b) M. D. Slater, D. Kim, E. Lee, C. S. Johnson, *Adv. Funct. Mater.* **2013**, *23*, 947–958; c) S.-W. Kim, D.-H. Seo, X. Ma, G. Ceder, K. Kang, *Adv. Energy Mater.* **2012**, *2*, 710–721.
[3] a) K. Share, A. P. Cohn, R. Carter, B. Rogers, C. L. Pint, *ACS Nano* **2016**, *10*, 9738–9744; b) Z. Jian, W. Luo, X. Ji, *J. Am. Chem. Soc.* **2015**, *137*, 11566–11569; c) Z. Xing, Y. Qi, Z. Jian, X. Ji, *ACS Appl. Mater. Interfaces* **2017**, *9*, 4343–4351.
[4] Y. Lu, Q. Zhang, L. Li, Z. Niu, J. Chen, *Chem* **2018**, *4*, 2786–2813.
[5] a) J. Yang, P. Xiong, Y. Shi, P. Sun, Z. Wang, Z. Chen, Y. Xu, *Adv. Funct. Mater.* **2020**, *30*,1909597; b) Z. Luo, L. Liu, Q. Zhao, F. Li, J. Chen, *Angew. Chem. Int. Ed. Engl.* **2017**, *56*, 12561–12565.
[6] a) S. N. Talapaneni, T. H. Hwang, S. H. Je, O. Buyukcakir, J. W. Choi, A. Coskun, *Angew. Chem. Int. Ed. Engl.* **2016**, *55*, 3106–3111; b) S. H. Je, H. J. Kim, J. Kim, J. W. Choi, A. Coskun, *Adv. Funct. Mater.* **2017**, *27*, 1703947.
[7] a) Y. Park, D. S. Shin, S. H. Woo, N. S. Choi, K. H. Shin, S. M. Oh, K. T. Lee, S. Y. Hong, *Adv. Mater.* **2012**, *24*, 3562–3567; b) J. Wang, H. Liu, C. Du, Y. Liu, B. Liu, H. Guan, S. Guan, Z. Sun, H. Yao, *Chem. Sci.* **2022**, *13*, 11614–11622; c) J. Wang, H. Liu, C. Du, X. Zhang, Y. Liu, H. Yao, Z. Sun, S. Guan, *Chem. Eng. J.* **2022**, *444*, 136598.
[8] a) C. M. Costa, E. Lizundia, S. Lanceros-Méndez, *Prog. Energy Combust. Sci.* **2020**, *79*, 100846; b) T. Janoschka, N. Martin, U. Martin, C. Friebe, S. Morgenstern, H. Hiller, M. D. Hager, U. S. Schubert, *Nature* **2015**, *527*, 78–81; c) I. Marriam, Y. Wang, M. Tebyetekerwa, *Energy Storage Mater.* **2020**, *33*, 336–359; d) L. Chen, J. L. Bao, X. Dong, D. G. Truhlar, Y. Wang, C. Wang, Y. Xia, *ACS Energy Lett.* **2017**, *2*, 1115–1121.
[9] a) J. Zhang, C. Ye, F. He, Y. Zeng, J. Xiao, X. Yang, H. Shu, H. Qi, W. Liu, P. Gao, *ChemSusChem* **2023**, *16*, e202202159; b) C. Wang, Y. Xu, Y. Fang, M. Zhou, L. Liang, S. Singh, H. Zhao, A. Schober, Y. Lei, *J. Am. Chem. Soc.* **2015**, *137*, 3124–3130.
[10] a) T. Cai, Y. Han, Q. Lan, F. Wang, J. Chu, H. Zhan, Z. Song, *Energy Storage Mater.* **2020**, *31*, 318–327; b) L. L. Jiang, C. Yan, Y. X. Yao, W. Cai, J. Q. Huang, Q. Zhang, *Angew. Chem. Int. Ed. Engl.* **2021**, *60*, 3402–3406.
[11] a) D. Han, Y. Han, J. Li, X. Liu, K. W. K. Yeung, Y. Zheng, Z. Cui, X. Yang, Y. Liang, Z. Li, S. Zhu, X. Yuan, X. Feng, C. Yang, S. Wu, *Appl. Catal. B* **2020**, *261*, 118248; b) T. Bessho, S. M. Zakeeruddin, C. Y. Yeh, E. W. G. Diau, M. Grätzel, *Angew. Chem. Int. Ed.* **2010**, *49*, 6646–6649.
[12] S. Grimme, J. Antony, S. Ehrlich, H. Krieg, *J. Chem. Phys.* **2010**, *132*, 154104.
[13] a) F. Xu, H. Xu, X. Chen, D. Wu, Y. Wu, H. Liu, C. Gu, R. Fu, D. Jiang, *Angew. Chem. Int. Ed. Engl.* **2015**, *54*, 6814–6818; b) H. Zhang, Y. Zhang, C. Gu, Y. Ma, *Adv. Energy Mater.* **2015**, *5*, 1402175.
[14] J. Yuan, B. Ren, X. Feng, P. Gao, E. Liu, S. Tan, *Chem. Commun. (Camb.)* **2020**, *56*, 5437–5440.
[15] a) Y. Tan, Z. Chen, Z. Tao, A. Wang, S. Lai, Y. Yang, *Angew. Chem. Int. Ed. Engl.* **2023**, *62*, e202217744; b) X. Han, S. Li, W. L. Song, N. Chen, H. Chen, S. Huang, S. Jiao, *Adv. Energy Mater.* **2021**, *11*, 2101446; c) E. Abouzari-Lotf, R. Azmi, Z. Li, S. Shakouri, Z. Chen, Z. Zhao-Karger, S. Klyatskaya, J. Maibach, M. Ruben, M. Fichtner, *ChemSusChem* **2021**, *14*, 1840–1846.
[16] a) B. Q. Li, S. Y. Zhang, L. Kong, H. J. Peng, Q. Zhang, *Adv. Mater.* **2018**, *30*, e1707483; b) X. Hu, J. Jian, Z. Fang, L. Zhong, Z. Yuan, M. Yang, S. Ren, Q. Zhang, X. Chen, D. Yu, *Energy Storage Mater.* **2019**, *22*, 40–47; c) L. Kong, B.-Q. Li, H.-J. Peng, R. Zhang, J. Xie, J.-Q. Huang, Q. Zhang, *Adv. Energy Mater.* **2018**, *8*, 1800849.
[17] T. Ma, Z. Pan, L. Miao, C. Chen, M. Han, Z. Shang, J. Chen, *Angew. Chem. Int. Ed. Engl.* **2018**, *57*, 3158–3162.
[18] H. Yang, S. Zhang, L. Han, Z. Zhang, Z. Xue, J. Gao, Y. Li, C. Huang, Y. Yi, H. Liu, Y. Li, *ACS Appl. Mater. Interfaces* **2016**, *8*, 5366–5375.
[19] Z. Lin, Z. M. Zhang, Y. S. Chen, W. Lin, *Angew. Chem. Int. Ed. Engl.* **2016**, *55*, 13739–13743.
[20] a) P. Gao, Z. Chen, Z. Zhao-Karger, J. E. Mueller, C. Jung, S. Klyatskaya, T. Diemant, O. Fuhr, T. Jacob, R. J. Behm, M. Ruben, M. Fichtner, *Angew. Chem. Int. Ed. Engl.* **2017**, *56*, 10341–10346; b) Y. Zeng, J. Zhou, J. Zhang, F. He, Y. Su, P. Wang, S. Tan, P. Gao, *Chem. Eng. J.* **2023**, *453*,139951; c) X. Feng, X. Wu, X. Chen, J. Yuan, S. Lv, B. Ren, X. Sun, E. Liu, S. Tan, P. Gao, *Energy Storage Mater.* **2021**, *42*, 454–463; d) Y. Sun, F. He, X. Huang, B. Ren, J. Peng, D. Chen, X. Hu, X. Sun, P. Gao, *Chem. Eng. J.* **2023**, *451*, 138734; e) X. Wu, X. Feng, J. Yuan, X. Yang, H. Shu, C. Yang, Z. liu, J. Peng, E. Liu, S. Tan, P. Gao, *Energy Storage Mater.* **2022**, *46*, 252–258.
[21] D.-Y. Wang, R. Liu, W. Guo, G. Li, Y. Fu, *Coord. Chem. Rev.* **2021**, *429*, 213650.
[22] X. Chen, X. Feng, B. Ren, L. Jiang, H. Shu, X. Yang, Z. Chen, X. Sun, E. Liu, P. Gao, *Nano-Micro Lett.* **2021**, *13*, 71.

Manuscript received: January 16, 2024
Revised manuscript received: March 6, 2024
Accepted manuscript online: March 10, 2024
Version of record online: March 26, 2024

© 2024 Wiley-VCH GmbH

25666223, 2024, 5, Downloaded from https://chemistry-europe.onlinelibrary.wiley.com/doi/10.1002/batt.202400031 by University of Ulsan, Wiley Online Library on [11/11/2025]. See the Terms and Conditions (https://onlinelibrary.wiley.com/terms-and-conditions) on Wiley Online Library for rules of use; OA articles are governed by the applicable Creative Commons License